Implications of Nanodevice Mobility on Terahertz Communication Links in the Human Vessels

Jorge Torres Gómez
TU Berlin, Germany
torres-gomez@ccs-labs.org

Johan Engstrand
Uppsala University, Sweden
johan.engstrand@angstrom.uu.se

Sergi Abadal
Universitat Politècnica de Catalunya, Spain
abadal@ac.upc.edu

Robin Augustine
Uppsala University, Sweden
robin.augustine@angstrom.uu.se

Thiemo Voigt
Uppsala University, Sweden
thiemo.voigt@angstrom.uu.se

Falko Dressler
TU Berlin, Germany
dressler@ccs-labs.org

ABSTRACT

This paper describes the time-varying nature of terahertz communication links between mobile nanodevices, targeting a realistic use case for nanodevice communication within human vessels. We consider a communication link through dipole-like nanoantennas, which flow and rotate in the bloodstream. Such a dynamic scenario causes random glitches in the received power level, resembling a fading-like channel. We present an analytic formulation for the time-variant impulse response and calculate performance metrics like the level crossing rate and the average fade duration. Our findings reveal crossings in the millisecond order and an average duration of fades on the same scale. Our study is the basis for designing robust decoders and error-correcting codes that mitigate the impact of variability on the received power level.

CCS CONCEPTS

• **Applied computing** → **Health informatics**; • **Hardware** → **Biology-related information processing**.

KEYWORDS

Terahertz, Nanoantenna, Human vessels, Time-varying channel

ACM Reference Format:

Jorge Torres Gómez, Johan Engstrand, Sergi Abadal, Robin Augustine, Thiemo Voigt, and Falko Dressler. 2024. Implications of Nanodevice Mobility on Terahertz Communication Links in the Human Vessels. In *The 11th Annual ACM International Conference on Nanoscale Computing and Communication (NANOCOM '24), October 28–30, 2024, Milan, Italy*. ACM, New York, NY, USA, 6 pages. https://doi.org/10.1145/3686015.3689351

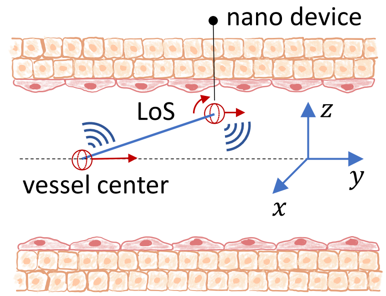

Figure 1: Mobility and rotation of nanodevices along vessel segments in the circulatory system.

1 INTRODUCTION

Electromagnetic (EM) waves in the terahertz (THz) band are enabling a multitude of new healthcare applications at the nanoscale. Examples are suppressing undesired interactions in proteins [2] and creating 3D images of red blood cells [6]. The THz nanocommunication systems also enable information transfer between nanodevices in the human body [9]. To that end, THz radio frequency (RF) front-ends are today conceived through plasmonic nanoantennas with dipole-like [8, 15], patch [16], and spiral geometry [3] designs.

A key aspect of the communication link between nanodevices is the time-varying nature of the channel in the human vessels. Nanodevices drifted by the bloodstream will experience a time-varying distance between each other. In addition, the nanoantennas may rotate, misaligning the transmitter and receiver radiation patterns; see Fig. 1. This dynamic position and rotation produce a fluctuating power level of the received signal, negatively affecting communication performance; which is yet to research.

Existing models for the in-body links predict the communication performance in the blood [7], but the time-varying nature of the channel has not been explored in detail. As we will show in this paper, when evaluating the communication link in the arterioles, the varying distance produces a variability of the received signal in a millisecond (ms) time-scale, while the rotation of the nanoantennas produces a much faster variability in the same time-scale. This variability will be reflected in the amplitude of the received signal, which will be observed as glitches falling below the receiver's sensitivity level. The impact of the blood flow dynamics on the communication link will, therefore, result in a fading-like channel impacting the communication performance.

Aiming at describing the communication link between nanodevices in the blood flow, this paper extends our previous researc in [17] to investigate the two most relevant related metrics regarding the channel time-variability: the level crossing rate (LCR) and

NANOCOM '24, October 28–30, 2024, Milan, Italy

ACM ISBN 979-8-4007-1171-8/24/10...$15.00
https://doi.org/10.1145/3686015.3689351

the average duration of fades; see [11, Sec. 4.7.3]. The LCR provides the frequency of crossings of the received power through the threshold sensitivity. When the received signal is below the receptor's sensitivity, the communication will be interrupted as the signal can no longer be decoded. Meanwhile, the average duration of fades provides the time duration of the interrupted link, where the received power is below the sensitivity of the receiver.

The presented study supports the further development of reliable communication schemes. As our findings illustrate, the channel resembles a fast-fading link, which requires implementing robust receptors to diminish the impact of fluctuations in the received signal level as in the case of mobile communications [1].

Our main contributions can be summarized as follows:

- We provide an analytic description for the time-varying channel in a link between two nanodevices that flow in the human vessels,
- we derive the theoretical calculations for the LCR and the average duration of fades, and
- we illustrate with realistic parameters the resulting LCR and average duration of fades. [1]

2 SYSTEM MODEL

Since we address an EM communication link in the blood vessels between two nanodevices, the system model includes mainly three components: (1) The RF front-end of the nanodevices, (2) the mobility of the nanodevices within the blood flow, and (3) the path loss attenuation within blood in the THz band. These components are described in the next subsections.

2.1 RF Front-End

The nanodevices are equipped with dipole-like nanoantennas following the design by Tamagnone et al. [15]. The nanoantenna comprises two radiator patches made of graphene and a substrate made of quartz with the dimensions listed in Table 1. [2] The design is shielded in a spheric cover made of polydimethylsiloxane (PDMS) with a radius $r = 35.7\,\mu\text{m}$. In our simulation in CST Studio Suite 2021, the shielded nanoantenna is surrounded by blood to evaluate the radiation pattern; see the complete design in Fig. 2 and further details in [17]. The resulting radiation pattern is illustrated in Fig. 3 yielding a gain in the range -40 to -12 dBi with a resonant frequency $f_c = 2.107$ THz.

2.2 Piezoelectric Nanogenerator

We evaluate the transmission power based on piezoelectric nanogenerator technologies, as reported in [10]. These nanogenerators harvest mechanical energy due to the contraction of ZnO nanowires produced by the interaction with pressure waveforms, like the ones in human vessels. This generator has a power density of $83\,\text{nW/cm}^2$, where we assume it is deployed along the bottom side of the cover surface in Fig. 2. This area is calculated as $A_g = 4\pi r^2/2 \approx 8 \times 10^{-9}\,\text{m}^2$. Following these calculations, the resulting transmitter power is $P_{\text{Tx}} = -90$ dBm. To cope with this low

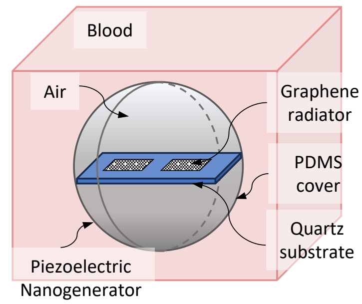

Figure 2: The antenna is modeled in CST as being shielded within a sphere made of biocompatible PDMS material, surrounded by blood.

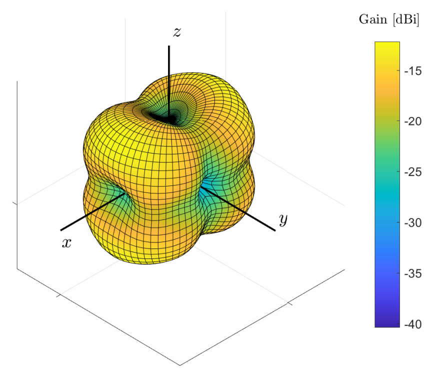

Figure 3: Radiation pattern of the nanoantenna inserted in blood.

power level at the receiver, we assume the lowest sensitivity level on wireless technologies for the nanosensor, as the case in global navigation satellite system (GNSS), which set a sensitivity value of -165 dBm as a requirement. [3]

2.3 Mobility Model for the Nanodevices

The mobility of the nanosensor will comprise two components: displacement and rotation. Regarding the displacement component, we assume the nanodevices travel in the arterioles, where the vessel thickness is $h_v = 200\,\mu\text{m}$ and the maximum speed is $v_c = 0.1$ cm/s along the vessel center; see [5, Table I]. In this mobility scenario, the spherical nanodevices will follow a straight path along the vessel stream, i.e., advection dominates diffusion. See this evaluation with the corresponding Péclet number in [17, Eq. (5)].

For simplicity and without loss of generalization, we assume the receiver node travels along the vessel center at the corresponding blood speed $v_c = 0.1$ cm/s. The transmitter node travels at $90\,\mu\text{m}$ away from the center and with initial distance $108\,\mu\text{m}$ away from the receiver. Along this vessel stream, the emitter travels at the less speed 0.02 cm/s; after evaluating [17, Eq. (3)]. Within this settings, the receiver will forward the transmitter position in the y-direction due to the larger traveling speed. Besides, for ease of calculation,

[1]We provide open access to the nanoantenna design in CST Studio Suite 2021 as well as the mobility model in Matlab 2023b code at https://github.com/jorge-torresgomez/terahertz_inbody

[2]Future work will evaluate other antenna's geomtries as listed in the Introduction.

[3]Future work will investigate the developments in nanoreceiver technologies in the THz band.

Table 1: Simulation parameters.

	Parameter	Description	Value
RF front end	f_c	Operating frequency	2.107 THz
	L	Graphene length	8.5 µm
	W	Graphene width	8 µm
	h	Graphene thickness	0
	E_F	Graphene chemical potential	0.6 ps
	τ	Graphene relaxation time	1 ps
	L_s	Substrate length	50 µm
	W_s	Substrate width	50 µm
	h_s	Substrate thickness	5 µm
		Quartz permittivity	3.75 F m
	G	Gap	2 µm
	$Z_{1,1}$	Antenna input impedance	324 Ω
	r	Shield inner radius	≈ 35.7 µm
		Shield thickness	0.1 µm
		PDMS permittivity	2.76 F/m
	P_{Tx}	Power of pulses	−73.9 dBm
	R_{th}	Receptor sensitivity	−165 dBm
Vessel	v_c	Blood speed in the vessel center	0.1 cm/s
	h_v	Vessel thickness	200 µm

[a] The inner radius of the shield is evaluated as $r^2 = \left(\frac{W_s}{2}\right)^2 + \left(\frac{L_s}{2}\right)^2 + h_s^2$.

we assume the center coordinates are on the vessel center and with the yz-plane in the plane of the two nanodevices; see Fig. 1.

Regarding the rotation component, due to the blood flow in the vessel, the emitter nanodevice will not only translate but also rotate with angular speed $\dot{\omega} \approx 6$ rad/s. This calculation is made with the flow's torque force while considering the nanodevice's moment of inertia, as described in [17, Sec. III B]. In this calculation, we also include the mass of the piezoelectric generator as $m_g \approx 6 \times 10^{-6}$ kg. This mass is evaluated as the product of the density of ZnO (nanowires) as 5.6×10^3 kg/m^3, [4] and the total volume. The total volume is calculated as the product of the total number of nanowires with the volume per nanowire as $\pi r_{\mathrm{ng}}^2 l_{\mathrm{ng}}$, where $r_{\mathrm{ng}} = 300$ nm is the radius (see [20]) and $l_{\mathrm{ng}} = 5$ µm is the length of the nanowire; see [10]. Finally, the total number of nanowires fitting on the generator's area (as $A_g \approx 8 \times 10^{-9}$ m^2) is evaluated in correspondence with the number of nanowires in 2 cm^2; which is reported as one million in [19]. This calculation yields $\left\lceil 8 \times 10^{-9} \frac{10^6}{2 \times 10^4} \right\rceil = 41$ nanowires, where $\lceil \cdot \rceil$ is the ceil operation.

Meanwhile, the nanodevice traveling in the vessel center will not experience the impact of the torque force, and consequently, it will not rotate and just follow the blood flow. We also assume that the initial orientations of both nanoantennas follows the uniform random distribution, and in any direction of space.

[4] Zinc oxide | 1314-13-2, https://www.chemicalbook.com/ChemicalProductProperty_EN_CB3853034.htm

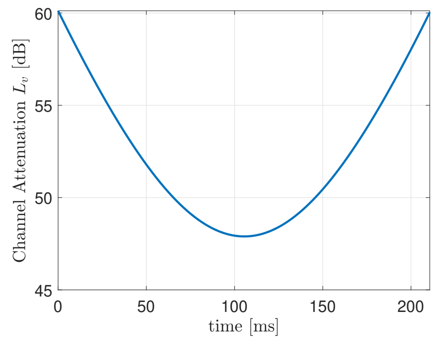

Figure 4: Channel path loss with time.

2.4 Path Loss Model

We model the channel path loss in the blood vessels using the varying distance $d(t)$ between nanodevices. As follows from [4], the path loss L_{v} is formulated with the spreading and molecular absorption loss (scattering loss is negligible) as

$$L_{\mathrm{v}}(t) = e^{-\mu_{\mathrm{abs}} d(t)} \frac{\lambda_{\mathrm{g}}}{\left(4\pi d(t)\right)^2}, \tag{1}$$

where $\mu_{\mathrm{abs}} = 4\pi n''/\lambda_{\mathrm{g}}$ is the molecular absorption coefficient, $d(t)$ is the distance between sender and receiver, and $\lambda_{\mathrm{g}} = \lambda/n'$ is the effective wavelength. The terms n' and n'' are the real and imaginary parts of the refractive index n of the medium the wave is traveling through (blood in our case). More detailed channel and dielectric characteristics of blood can be found in [12, 14].

Considering the initial position of the emitter and receiver nodes (see Fig. 1); the evaluation of Eq. (1) produces the curve illustrated in Fig. 4. The resulting path loss is in the range 47 to 60 dB, with a minima where the distance between the emitter and receiver is the shortest.

3 TIME-VARIANT IMPULSE RESPONSE

The communication link between the two nanodevices will be impacted by the varying distance between them and by the transmitting nanoantenna's rotation. We account for this mobility with the baseband received signal formulation as (see [18, Sec. 2.2.2])

$$y_{\mathrm{b}} = \int_{-\infty}^{\infty} h_{\mathrm{b}}(\tau, t) x_{\mathrm{b}}(t - \tau)\, \mathrm{d}\tau, \tag{2}$$

where [18, Eq. (2.28)]

$$h_{\mathrm{b}}(\tau, t) = a(t) e^{-2\pi f_c \tau(t)} \delta(t - \tau(t)), \tag{3}$$

is the time-varying channel impulse response. To evaluate $h(\tau, t)$, the value of $\tau(t) = \frac{d(t)}{c/n'} \sim 0.6$ fs represents the propagation delay in the link, which is almost negligible, c is the speed of light, c/n' is the waveform speed in blood, n' is the real part of the refractive index of blood, and $d(t) = |\mathrm{Tx}_{\mathrm{pos}} - \mathrm{Rx}_{\mathrm{pos}}|$ is the time-varying distance between the transmitter and the receiver. The term $a(t)$ stands for the time-varying amplitude in the link and is evaluated as

$$a(t) = \sqrt{\frac{g_{\mathrm{Tx}}(t) \times g_{\mathrm{Rx}}(t)}{L_{\mathrm{v}}(t)}}, \tag{4}$$

where $g_{\mathrm{Tx}}(t)$ is the transmitter's gain, $g_{\mathrm{Rx}}(t)$ is the receiver's gain, and are evaluated with the radiation pattern $G(\theta, \phi)$ in Fig. 3, where θ is the elevation angle, and ϕ is the azimuth coordinate. The value of $L_v(t)$ is the path loss in the channel as given with Eq. (1).

The transmitter and receiver's gain are evaluated according to the rotation and displacement of the antennas, as produced by the fluid; see Fig. 1. Both gains must be evaluated in the line of sight (LoS) link between both devices, as represented with the blue line in Fig. 1. Here, we assume a neglible impact of reflections in the vessel walls due to the larger path loss. As for the receiver's gain, the evaluated gain will be given by the elevation and azimuth angles, as given by the LoS direction with the receiver, yielding

$$g_{\mathrm{Rx}}(t) = G(\theta_{\mathrm{Rx,init}} + \theta_{\mathrm{Rx}}(t), \phi_{\mathrm{Rx,init}} + \phi_{\mathrm{Rx}}) \tag{5}$$

where the values of $\theta_{\mathrm{Rx,init}}$ and $\phi_{\mathrm{Rx,init}}$ refer to the initial orientation of the antenna, which we assume to follow a random variable with uniform distribution in the range $[-\pi,\ \pi]$. The value of θ_{Rx} and ϕ_{Rx}, which refer to the LoS link with the trasmitter,are evaluated while transforming the cartesian coordinates for the LoS direction to the spherical coordinates as follow

$$\begin{aligned} \theta_{\mathrm{Rx}}(t) &= \tan^{-1} \frac{\mathrm{Tx}_{\mathrm{pos}z}}{|\mathbf{Tx}_{\mathrm{pos}}(t) - \mathbf{Rx}_{\mathrm{pos}}(t)|}, \\ &= \tan^{-1} \frac{\mathrm{Tx}_{\mathrm{pos}z}}{\sqrt{(\mathrm{Tx}_{\mathrm{pos}y,0} + (v(\mathrm{Tx}_{\mathrm{pos}z}) - v_{\mathrm{c}}) \times t)^2 + \mathrm{Tx}_{\mathrm{pos}z}^2}}, \\ \phi_{\mathrm{Rx}} &= \tan^{-1} \frac{\mathrm{Tx}_{\mathrm{pos}y}(t) - \mathrm{Rx}_{\mathrm{pos}y(t)}}{\mathrm{Tx}_{\mathrm{pos}x} - \mathrm{Rx}_{\mathrm{pos}x}} = \frac{\pi}{2}. \end{aligned} \tag{6}$$

In the above relations, the azimuth component (ϕ) evaluates as $\frac{\pi}{2}$ as both antennas are moving in the yz-plane. As for the elevation component (θ), the denominator evaluates the distance with the transmitter and receiver coordinates denoted with the vectors $\mathbf{Tx}_{\mathrm{pos}}(t)$ and $\mathbf{Rx}_{\mathrm{pos}}(t)$, respectively. Along the y-axis the transmitter location will be given by $v_{\mathrm{c}} \times t$, and the transmitter location as $(\mathrm{Tx}_{\mathrm{pos}y,0} + v(\mathrm{Tx}_{\mathrm{pos}z}) \times t)$, where $v(\mathrm{Tx}_{\mathrm{pos}z})$ is evaluated with [17, Eq. (3)], and $\mathrm{Tx}_{\mathrm{pos}y,0}$ is the initial position of the emitter in the y-axis. Along the z-axis, the transmitter coordinate is constant as $\mathrm{Tx}_{\mathrm{pos}z}$, while the receiver is zero. In these relations, we implicitly assume that the system coordinates are centered at the initial receiver coordinates and the z-axis oriented in the plane where the transmitter is moving, see Fig. 1.

As for the transmitter, the displacement and the rotation will significantly modify the time evolution of the gain. Similarly to the receiver, we evaluate the gain having the initial angle and the time-evolution of the elevation and azimuth angles as follows

$$g_{\mathrm{Tx}}(t) = G\big(\theta_{\mathrm{Tx,init}} + \theta_{\mathrm{Tx}}(t), \phi_{\mathrm{Tx,init}} + \phi_{\mathrm{Tx}}\big), \tag{7}$$

where

$$\begin{aligned} \theta_{\mathrm{Tx}}(t) &= \tan^{-1} \frac{\mathrm{Tx}_{\mathrm{pos}z}}{|\mathbf{Tx}_{\mathrm{pos}}(t) - \mathbf{Rx}_{\mathrm{pos}}(t)|} + \pi - \dot{\omega} \times t, \\ &= \tan^{-1} \frac{\mathrm{Tx}_{\mathrm{pos}z}}{\sqrt{(\mathrm{Tx}_{\mathrm{pos}y,0} + (v(\mathrm{Tx}_{\mathrm{pos}z}) - v_{\mathrm{c}}) \times t)^2 + \mathrm{Tx}_{\mathrm{pos}z}^2}} \\ &\quad + \pi - \dot{\omega} \times t, \\ \phi_{\mathrm{Tx}} &= \tan^{-1} \frac{\mathrm{Rx}_{\mathrm{pos}y} - \mathrm{Tx}_{\mathrm{pos}y}}{\mathrm{Rx}_{\mathrm{pos}x} - \mathrm{Tx}_{\mathrm{pos}y}} = \frac{\pi}{2}. \end{aligned} \tag{8}$$

In this evaluation, the azimuth component (ϕ_{Tx}) also evaluates as $\frac{\pi}{2}$ as the transmitter is moving in the yz-plane. As for the elevation component ($\theta_{\mathrm{Tx}}(t)$), the expression includes the time-varying distance between the emitter and the receiver with the term $(|\mathbf{Tx}_{\mathrm{pos}}(t) - \mathbf{Rx}_{\mathrm{pos}}(t)|)$. Besides, in contrast to the receiver, this expression also includes the rotation produced by the fluid with the term $\dot{\omega} \times t$. [5] We include this term with a negative sign to follow the clockwise direction of the rotation. Finally, we add the constant π, evaluating the direction from the emitter to the receiver.

Following Equations (6) and (8), the transmitter and receiver gains will be impacted not only by the time-varying distance between the emitter and the receiver but also by its antenna orientation. To illustrate this variability, Fig. 5a depicts the receiver gain with time and for various initial angles along the three axes. The time evolution of the gain will be highly dependent on the initial angle for the nanoantenna. The degree of variability of the transmitter gain with time is in the order of ms, as it is impacted by the blood fluid speed, which is in the magnitude's order of cm/s; see Table 1. The transmitter gain exhibits a more speedy variability in the same order's magnitude of the ms, which is due to the rotation and the variability of the radiation pattern surface; see the evaluation with Fig. 5b.

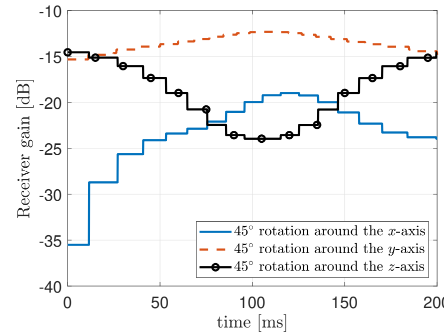

(a) Receiver gain for various initial angles

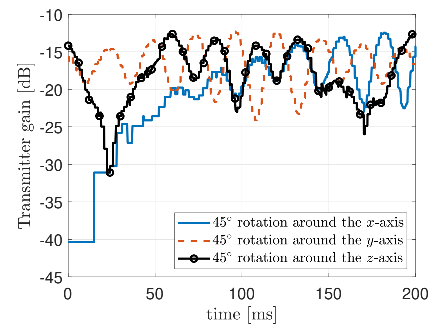

(b) Transmitter gain for various initial angles

Figure 5: Receiver and transmitter gains for various initial angles.

[5] Note that the rotation term does not appear with the receiver formulation in Eq. (6), since it travels in the vessel center, where the torque force is zero.

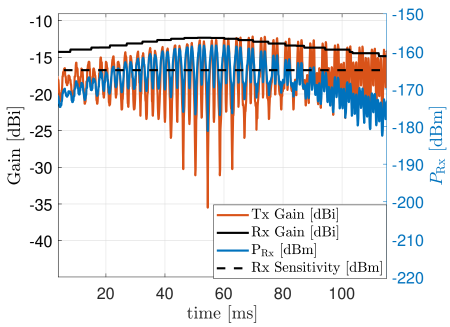

Figure 6: Received power and antenna gain over time as the nanoantennas flow with the blood.

4 LEVEL CROSSING RATE AND AVERAGE FADE DURATION

The variability of the channel amplitude with time induces the amplitude variability of the received signal. To illustrate, Fig. 6 depicts the variability of the transmitter and receiver gain, as well as the received power. As a result of this variability, the received power level is

$$P_{\mathrm{dB}}(t) = P_{\mathrm{Tx}} + G_{\mathrm{Tx,dB}}(t) + G_{\mathrm{Rx,dB}}(t) - L_{\mathrm{v,dB}}(t), \tag{9}$$

which is also dependent on the mobility and rotation of antennas. The amplitude of the received signal resembles small-scale fading as its level abruptly falls below the receiver sensitivity value.

To account for the quality of the communication link, in this section, we develop the LCR and the average fade duration in the link; see [11, Sec. 4.7.3]. The LCR refers to the average number of times when the power level crosses a given sensitivity value, here denoted as R_{th}, and calculated as [13, Eq. (4.1)]

$$N_R(t) = \int_0^{\infty} \dot{r} p\{R_{\mathrm{th}}, \dot{r}, t\}\, \mathrm{d}\dot{r}, \tag{10}$$

along the time interval $[t,\ t + \mathrm{d}t]$, where $\dot{r}$ is the time derivative of the received power, and $p(\dot{r}, R_{\mathrm{th}}, t)$ is the joint Probability Density Function (PDF) of $\dot{r}$ and the received power level r at $r = R_{\mathrm{th}}$.

We evaluate $p\{R_{\mathrm{th}}, \dot{r}, t\}$ numerically, and mostly accounting for the impact of the transmitter variability. As depicted in Fig. 5, the variability of the transmitter gain is faster than the emitter and the channel path loss in Fig. 4. Under these assumptions, we calculate $\dot{r}$ as

$$\dot{r}(t) \approx \frac{1}{\Delta t} \frac{\mathbb{E}\{g_{\mathrm{Rx}}(t)\}}{L_{\mathrm{v}}(t)} \left(g_{\mathrm{Tx}}(t + \Delta t) - g_{\mathrm{Tx}}(t)\right), \tag{11}$$

with $r = a^2(t)$ (see Eq. (4)), assuming $g_{\mathrm{Rx}}(t + \Delta t) \approx g_{\mathrm{Rx}}(t)$ and $L_{\mathrm{v}}(t + \Delta t) \approx L_{\mathrm{v}}(t)$, when Δt is in the ns scale. Besides, we evaluate the expected average for the receiver gain to account for all possible initial orientation angles. This expected value (≈ -18.4 dBi) is evaluated numerically with the histogram of values for the radiation pattern $G(\theta, \phi)$; see Fig. 7.

We compute the difference $(g_{\mathrm{Tx}}(t+\Delta t) - g_{\mathrm{Tx}}(t))$ first calculating the $g_{\mathrm{Tx}}(t)$ value that evaluates the threshold level R_{th} in the received power. We calculate $g_{\mathrm{Tx}}(t) = g_{\mathrm{Tx,th}}$ equating $P_{\mathrm{dB}}(t) = R_{\mathrm{th}}$ in Eq. (9) and also evaluating $G_{\mathrm{Rx,dB}}(t)$ with its expected value (≈ -18 dB). From this point in the radiation pattern surface, we evaluate all the possible other points $g_{\mathrm{Tx}}(t + \Delta t)$ from $g_{\mathrm{Tx,th}}$. We assume all these points are those with elevation angles at $\Delta\theta = \dot{\omega} \times \Delta T$ [rad]

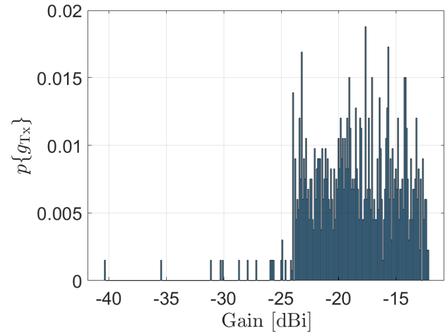

Figure 7: Numerical evaluation of the probability $p\{g_{\mathrm{Tx}}\}$

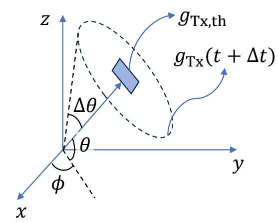

Figure 8: Illustration of gain values around the threshold gain $g_{\mathrm{Tx,th}}$.

from $g_{\mathrm{Tx,th}}$, as we assume the arbitrary orientation of the initial antenna position, see an illustration in Fig. 8. From this specific value, other reachable points will be located in the range −22 to −18 dBi. Following this sequence of points for $g_{\mathrm{Tx}}(t + \Delta t)$, we evaluate the histogram to estimate $p\{R_{\mathrm{th}}, \dot{r}, t\}$ numerically.

Once the LCR metric is calculated with Eq. (10), the average duration of fading is readily evaluated as [11, Eq. (4.81) pp. 186]

$$\mathbb{E}\{\tau\} = \frac{1}{N_R} p\{r < R_{\mathrm{th}}\}, \tag{12}$$

where $p\{r < R_{\mathrm{th}}\}$ is the probability that the received power level is less than the receptor's sensitivity, here denoted as R_{th}. We evaluate this probability with a similar procedure as for the LCR with the histogram of values in the antenna gain. We find the minimum value of the transmitter gain $g_{\mathrm{Tx,th}}$ that fulfills $P_{\mathrm{dB}}(t) = R_{\mathrm{th}}$. Then, we numerically evaluate the integral $\int_0^{g_{\mathrm{Tx,th}}} P(g)\, \mathrm{d}g$ as a result of the probability $p\{r < R_{\mathrm{th}}\}$, where $P(g)$ is estimated with the histogram of values for the antenna gain.

5 RESULTS

This section illustrates the two performance metrics, LCR and the average fade duration, with the nanodevice's position. We develop their numerical calculation with the description given in Section 4. In this evaluation, we consider that $t = 0$ refers to the case for the initial position of the transmitter and receiver nanodevices, where the emitter is at a forward position, as illustrated in Fig. 1. As time increases, the receiver moves faster as it travels through the vessel center; thereby, the channel path loss also decreases with time until it increases again when the receiver forwards the emitter node; see Fig. 4 for the time evolution of the path loss.

In the vicinity of the minimum path loss, we found the LCR around the 200 crossings/ms. Once the LCR is calculated, the average duration of fades is numerically evaluated with Eq. (12). The

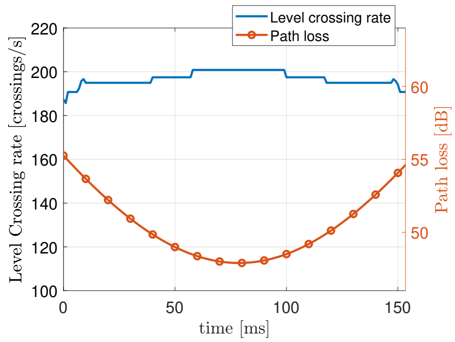

(a) Level crossing rate versus time.

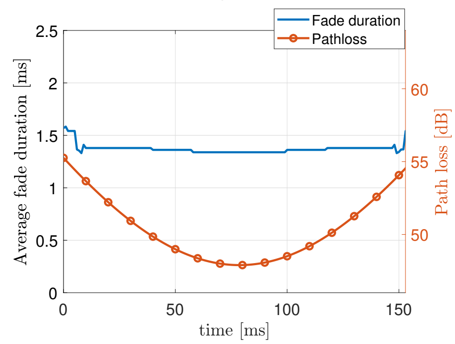

(b) Average fade duration versus time.

Figure 9: LCR and average fade duration metrics.

average duration of fades is illustrated in Fig. 9b, where the duration of fades is around 1.5 ms. The results in Fig. 9a characterize a medium- to fast-fading channel when the pulse emission is performed with a bandwidth in the order of the MHz. For this emission rate, there is one observed glitch per received pulse on average. Besides, according to the results in Fig. 9b, this channel characterizes a large-scale fade-like when the duration of pulses is less than ms scale. Due to these results, such a communication link would require designing receivers while including a channel estimator component, so to avoid emissions during the fading time-interval.

6 CONCLUSION

In this paper, we assessed the time-varying communication link between nanodevices moving in the human circulatory system. The analytical expressions introduced in this paper target a realistic link as we now also include in the radiation pattern of nanoantennas inserted in blood and the impact of mobility. We observed a medium to fast-fading channel in the THz band and also a large-scale fading behavior when performing emissions at a MHz rate and with a pulse duration in the ns scale. This eventually demands channel compensation mechanisms to neglect the impact of glitches in the received sequence and robust schemes to overcome large-scale fading. The methodology introduced can be straightforwardly extended to other antenna designs and mobility scenarios in the vessel segments, which is part of our future research directions.

ACKNOWLEDGMENTS

This work was supported in part by the project IoBNT, funded by the German Federal Ministry of Education and Research (BMBF) under grant number 16KIS1986K, and by the project NaBoCom, funded by the German Research Foundation (DFG) under grant number DR 639/21-2.

REFERENCES

[1] Alexandra Duel-Hallen, Shengquan Hu, and H. Hallen. 2000. Long-range prediction of fading signals. *IEEE Signal Processing Magazine* 17, 3 (May 2000), 62–75. https://doi.org/10.1109/79.841729

[2] Hadeel Elayan, Andrew W. Eckford, and Raviraj S. Adve. 2023. Terahertz Induced Protein Interactions in a Random Medium. *IEEE Transactions on Molecular, Biological and Multi-Scale Communications* 9, 4 (Dec. 2023), 435–446. https://doi.org/10.1109/tmbmc.2023.3327302

[3] Hadeel Elayan, Raed M. Shubair, Josep Miquel Jornet, Asimina Kiourti, and Raj Mittra. 2018. Graphene-Based Spiral Nanoantenna for Intrabody Communication at Terahertz. In *IEEE International Symposium on Antennas and Propagation and National Radio Science Meeting (AP-S/URSI 2018)*. IEEE, Boston, MA. https://doi.org/10.1109/apusncursinrsm.2018.8608890

[4] Hadeel Elayan, Raed M. Shubair, Josep Miquel Jornet, and Raj Mittra. 2017. Multi-layer Intrabody Terahertz Wave Propagation Model for Nanobiosensing Applications. *Elsevier Nano Communication Networks* 14 (Dec. 2017), 9–15. https://doi.org/10.1016/j.nancom.2017.08.005

[5] Matthieu Fruchard, Laurent Arcese, and Estelle Courtial. 2014. Estimation of the Blood Velocity for Nanorobotics. *IEEE Transactions on Robotics and Automation* 30, 1 (Feb. 2014), 93–102. https://doi.org/10.1109/tro.2013.2288799

[6] Hipolito Gomez-Sousa, Oscar Rubinos-Lopez, and Jose Angel Martinez-Lorenzo. 2016. Hematologic characterization and 3D imaging of red blood cells using a Compressive Nano-antenna and ML-FMA modeling. In *10th European Conference on Antennas and Propagation (EuCAP 2016)*. IEEE, Davos, Switzerland. https://doi.org/10.1109/eucap.2016.7481922

[7] Ratna Indrawijaya and Thomas Kürner. 2018. Simulation of Terahertz Intrabody Wireless Nano Sensor Networks in the Presence of Noise and Interference. In *12th European Conference on Antennas and Propagation (EuCAP 2018)*. IET, London, United Kingdom. https://doi.org/10.1049/cp.2018.1271

[8] Josep Miquel Jornet and Ian F. Akyildiz. 2010. Graphene-based nano-antennas for electromagnetic nanocommunications in the terahertz band. In *4th European Conference on Antennas and Propagation (EuCAP 2010)*. EurAAP, Barcelona, Spain, 1–5.

[9] Filip Lemic, Sergi Abadal, Wouter Tavernier, Pieter Stroobant, Didier Colle, Eduard Alarcon, Johann M. Marquez-Barja, and Jeroen Famaey. 2021. Survey on Terahertz Nanocommunication and Networking: A Top-Down Perspective. *IEEE Journal on Selected Areas in Communications* 39, 6 (June 2021), 1506–1543. https://doi.org/10.1109/jsac.2021.3071837

[10] Jin Liu, Peng Fei, Jun Zhou, Rao Tummala, and Zhong Lin Wang. 2008. Toward high output-power nanogenerator. *Applied Physics Letters* 92, 17 (4 2008). https://doi.org/10.1063/1.2918840

[11] Theodore S. Rappaport. 1996. *Wireless Communications: Principles and Practice.* Prentice Hall.

[12] C. B. Reid, G. Reese, A. P. Gibson, and V. P. Wallace. 2013. Terahertz Time-Domain Spectroscopy of Human Blood. *IEEE Journal of Biomedical and Health Informatics* 17, 4 (July 2013), 774–778. https://doi.org/10.1109/jbhi.2013.2255306

[13] Steven O Rice. 1948. Statistical Properties of a Sine Wave Plus Random Noise. *Bell System Technical Journal* 27, 1 (Jan. 1948), 109–157.

[14] Jennifer Simonjan, Bige Deniz Unluturk, and Ian F. Akyildiz. 2022. In-body Bionanosensor Localization for Anomaly Detection via Inertial Positioning and THz Backscattering Communication. *IEEE Transactions on NanoBioscience* 21, 2 (April 2022), 216–225. https://doi.org/10.1109/tnb.2021.3123972

[15] M. Tamagnone, J. S. Gómez-Díaz, J. R. Mosig, and J. Perruisseau-Carrier. 2012. Reconfigurable terahertz plasmonic antenna concept using a graphene stack. *Applied Physics Letters* 101, 21 (Nov. 2012). https://doi.org/10.1063/1.4767338

[16] Anand Sreekantan Thampy, Mayur Sudesh Darak, and Sriram Kumar Dhamodharan. 2015. Analysis of graphene based optically transparent patch antenna for terahertz communications. *Physica E: Low-dimensional Systems and Nanostructures* 66 (Feb. 2015), 67–73. https://doi.org/10.1016/j.physe.2014.09.023

[17] Jorge Torres Gómez, Jennifer Simonjan, Johan Engstrand, Sergi Abadal, Robin Augustine, Thiemo Voigt, and Falko Dressler. 2024. Mobility Matters at Nanoscale: Rendering the Received Terahertz Signal Power in Human Blood Vessels. In *7th IEEE International Balkan Conference Communications and Networking (BalkanCom 2024)*. IEEE, Ljubljana, Slovenia. to appear.

[18] David Tse and Pramod Viswanath. 2005. *Fundamentals of Wireless Communication.* Cambridge University Press. https://doi.org/10.1017/CBO9780511807213

[19] Xudong Wang, Jin Liu, Jinhui Song, and Zhong Lin Wang. 2007. Integrated Nanogenerators in Biofluid. *Nano Letters* 7, 8 (6 2007), 2475–2479. https://doi.org/10.1021/nl0712567

[20] Sheng Xu, Benjamin J. Hansen, and Zhong Lin Wang. 2010. Piezoelectric-nanowire-enabled power source for driving wireless microelectronics. *Nature Communications* 1, 1 (10 2010). https://doi.org/10.1038/ncomms1098